Subtomogram averaging reveals *in situ* structure of dimeric hibernating ribosomes in archaea

Vera van Schijndel[1*]

23-6-2022

Supervised by W. (Wenfei) Song[2] and M.L. (Marten) Chaillet Msc[2]
Examined by Prof. dr. F.G. (Friedrich) Förster[2] and Dr. S.C. (Stuart) Howes[2]

[1] Molecular and cellular life sciences master's program, Graduate School of Life Sciences, Utrecht University, 3584 CH Utrecht, The Netherlands – Student no. 6091326

[2]Structural Biochemistry & Biophysics, Bijvoet Center for Biomolecular Research, Department of Chemistry, Faculty of Science, Utrecht University, 3584 CH Utrecht, The Netherlands

[*]correspondence: v.vanschijndel@students.uu.nl

Abstract

Protein synthesis, one of the most important cellular processes, is carried out by ribosomes. In response to various stress conditions, cell synthesis is supressed by the formation of functionally inactive ribosomes. The stage in the ribosome cycle at which the ribosome loses translational activity is referred to as 'Hibernation'. The process of ribosome hibernation is well studied in bacteria, whereas not so much is known about the process in eukaryotes. A better understanding of ribosome hibernation in archaeal cells could help to learn more about the evolutionary history of this process, however, ribosome hibernation in archaea has not been studied before. Here we investigated hibernating ribosomes from the hyperthermophilic archaeon *Pyrococcus furiosus in situ* using cryo-electron tomography (cryoET). Using an advanced subtomogram averaging workflow, we show that approximately 10% of ribosomes form dimeric structures in the stationary phase. We demonstrate that dimeric ribosomes are in a single conformation, while monosomes adopt various conformations. In summary, we revealed the first native hibernating ribosome dimer structure from archaea.

Introduction

Cellular protein synthesis is carried out by the ribosome, which is a highly conserved RNA-protein complex. It consists of two ribonucleoprotein subunits, one of which is about twice the size of the other. The small subunit (SSU) facilitates decoding of the messenger RNA (mRNA). The large subunit (LSU) contains the peptidyl transferase centre (PTC), which mediates the formation of peptide bonds in the nascent protein[1]. The mechanism of protein synthesis can be described in four distinct phases: First, the small ribosomal subunit binds to the mRNA and upon recognition of an initiator codon, the large ribosomal subunit is recruited to form a 70S (80S in eukaryotes) ribosome; Second, aminoacyl-tRNAs deliver amino acids, which are incorporated into the elongating polypeptide chain by the formation of peptide bonds; Third, the polypeptide is released upon recognition of a stop codon on the mRNA; Fourth, ribosomes split into free subunits that can be recycled to continue translation of other mRNAs[2,3].

In this research we focus on the native structure of ribosomes in archaea in stationary phase. Archaea are a kingdom of single-celled prokaryotic organisms with molecular characteristics that separates them from bacteria. The cytological properties of bacteria and archaea are relatively simple, whereas eukaryotes are characterized by a high degree of cellular complexity. Comparison of genes among bacteria, archaea and eukaryotes showed that they were more similar between eukaryotes and archaea, suggesting that eukaryotes have likely evolved from archaea[4]. The general principles of mechanisms involving ribosomes are the same in the three domains of life, however the molecular mechanisms are different in bacteria, eukaryotes, and archaea and may also vary depending on the mRNA. For example, in eukaryotes, translation initiation is more complicated with many initiation factors involved[5], whereas archaeal translation is less complicated with some initiation factors corresponding to a subset of eukaryotic translation factors[6,7].

A 6.6Å resolution ribosome structure has previously been achieved in *Pyrococcus furiosus* using single particle analysis[8]. This technique relies on homogeneous samples of ribosomes. Higher order structures such as polysomes display a degree of plasticity in their molecular organisation which makes them intractable to single particle analysis. Cryo-electron tomography (CET)[9] overcomes this limitation by allowing the visualization of macromolecular structures in *situ*.

Protein synthesis is one of the most energy demanding processes in the cell[10]. Therefore it is important that cells can regulate protein synthesis under different conditions. In the exponential (log) phase, cells are actively translating various proteins, while many ribosomes go into hibernation in the stationary phase. When cells enter the stationary phase, many ribosomes go into hibernation in which ribosomal biosynthesis as well as protein synthesis is supressed[11–13]. This event is mediated by hibernation factors which inactivate ribosomes by locking individual

ribosomes in an inactive site or through the promotion of the formation of dimeric, 100S ribosomes[14]. In bacteria, the proteins ribosome modulation factor (RMF), hibernation promoting factor (HPF), ribosome associated inhibitor (RaiA) and ribosome associated factor Y (YfiA) regulate the ribosome hibernation process[15,16]. Structural studies on the native state of ribosomal dimers (100S) from *E.coli* cells in stationary phase revealed that ribosome dimers are associated via their small (30S) subunits and that this conformation is different than from stalled polysomes[17,18].

The mechanism of ribosome hibernation is less studied in eukaryotes. Ribosomal hibernation factors have so far been characterized at the single (80S) ribosome level. The first eukaryotic hibernation factor, suppressor of target of Myb protein 1 (Stm1; SERPINE1 mRNA-binding protein 1 [SERBP1] in mammals), was found in stressed yeast cells and binds to the mRNA entry channel, thereby occupying the active sites of the ribosome[19]. Furthermore, late-annotated short open reading frame2 (Lso2; coiled-coil domain containing short open reading frame 124 [CCDC124] in mammals) was found to sequester the mRNA binding pocket as well as the polypeptide exit tunnel[20,21]. The mammalian equivalent of the previously described bacterial dimer, a dimer of 80S monomers (110 complex), has been observed in rat C6 glioma cells under stress conditions. Polysome profiles suggested that the population of rat 110S ribosomes consist of 80S dimers and 60-80S heterodimers[22]. A more recent study revealed a unique structure of a dimeric hibernating ribosome from a eukaryotic intracellular pathogen, which is clearly distinct from bacterial disomes[23].

Here, we use an advanced subtomogram averaging workflow to investigate the structure of archaeal ribosomes of cells which are in stationary phase (Fig. S1). Our results reveal that a subset of ribosomes form hibernating ribosome dimers in *Pyrococcus furiosus*. We demonstrated that dimeric ribosomes are in a single conformation, while monosomes adopt various conformations. The structure of these dimers has been characterized for the first time in archaea. We saw that, like in bacteria, ribosome dimers are associated via their small ribosomal subunits.

Methods

Monitoring *Pyrococcus furiosus growth curve*

A *P. furiosus* cell culture was incubated at 90 °C. Every hour 10mL was taken from the cell culture using a syringe into a 15mL tube and centrifuged at 500g for 10 minutes. The pellet was then resuspended and pipetted into a 1mL tube. The optical density (OD) was measured to estimate the growth of the cells using a spectrometer with a light source of 600nm. These steps were repeated for 21 hours.

Data collection and tomogram reconstruction

Tiltseries were acquired on a 200-kV Talos Arctica (Thermo Fisher Scientific) equipped with a direct electron detector K2 camera (3838x3710 pixel). The pixel size corresponds to 2.17 Å or 1.734 Å on the specimen level. Data acquisition was performed with the SerialEM software[24]. A defocus range of 3 µm to 8 µm was used. A tilt range of approximately -60° to +60° with 2° or 3° steps was used for data collection with total dose of approximately 80-120 $e^-/Å^2$. Correction of electron beam-induced sample motion was performed using MotionCor2[25]. Tomograms were reconstructed using IMOD[26] (version 4.10.49) package; The tilt series were aligned using fiducial model generation. Contrast transfer function (CTF) correction was performed and tomograms were reconstructed using weighted back projection. The tomograms were binned 8 times to a pixel size of 17.4 Å or 13.9 Å.

Template matching

Template matching was performed using the software package PyTom[27] (version 0.993). The 3D template was generated from 6.6 Å resolution ribosome structure from *P. furiosus* (PDB entry 4V6U)[8]. The template was generated using the template_generation.py script (script S1). The template was non-mirrored and a mask of size 26 pixels with a radius of 10 pixels and a smoothing factor of 2 was used. A job was made using the localization.py script for the localization of the structures in the tomogram. The cross-correlation function was calculated by rotating the template in different orientations. Finally, the particle list was generated using the extractCandidates.py command. The particles were manually inspected using the PyTom GUI and unwanted particles were deselected. 6407 particles were identified as bona fide ribosomes. Subtomograms were reconstructed using WARP[28] and binned to a pixel size of 4.43 Å and 13.02 Å with a box size of 100 pixels.

Image processing

Image processing was performed using RELION[29] (version 3.1.1) The dataset of 6407 particles were aligned in a completely unsupervised manner using a reference-free refinement from 3D images. The initial model was refined with an initial low pass filter of 50 Å during 25 iterations with an initial angular sampling rate of 7.5 degrees. Further 3D classification was performed using masks generated by the relion_mask_create command. Particles belonging to a well-defined class were retained and refined during 25 iterations. Finally, the particles belonging to these classes were processed to obtain final density according to the 0.143 FSC gold-standard criterion.

Figure generation

Figures showing electron densities and atomic models were generated using UCSF Chimera[30]. The ribosome model of *P. furiosus* (PDB entry 46VU)[8] was fitted into our density using the UCSF Chimera "Fit in map" tool. The density map EMD-3638 was used for the comparison with hibernating dimeric ribosome from *S. aureus*, EMD-3664 for *S. subtilis* and EMD-5174 for *E.coli*. The maps were resized to a pixel size of 13.02 Å and a box size of 100 pixels using the RELION[29] "relion_image_handler" tool. The comparison was made by aligning one ribosome of each map to one ribosome of the *P. furiusus* dimeric ribosome map.

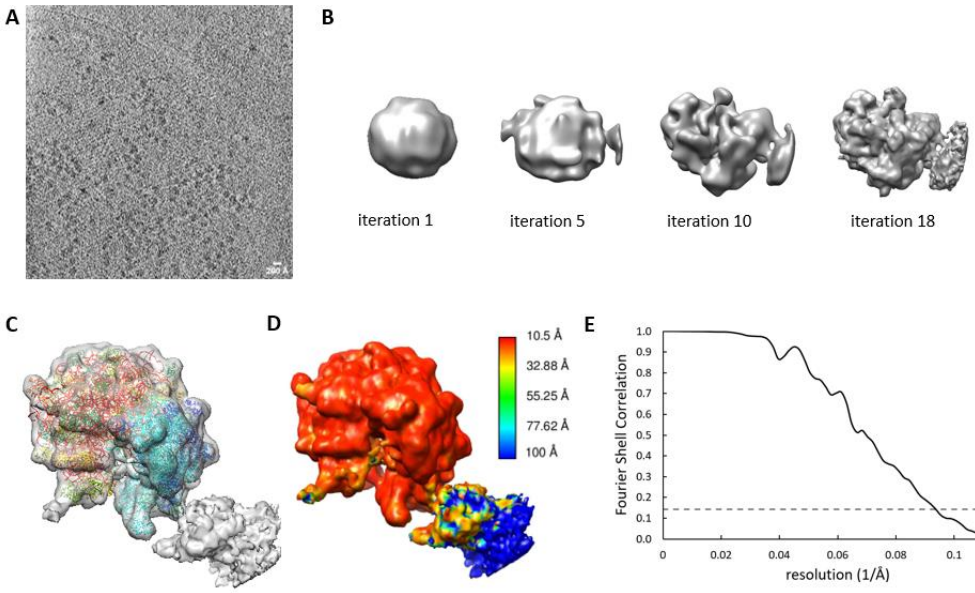

Figure 1, Refinement of 70S ribosomes. *A. slice of a bin 8 tomogram. Scale bar: 200 Å. B. Isosurface representation of 3D maps obtained during iterative reference-free alignment of 6,407 subtomograms. Iteration 1 corresponds to the initial reference that was obtained by averaging over all subtomograms in random orientations. C. 4,594 subtomograms depicting 70S ribosomes were aligned using simultaneous translational and restricted rotational search in real space. D. Local resolution map depicting the local resolution according to the colour bar. Low resolution is observed of the extra density part. E. Fourier shell correlation of the 10.7 Å density map. The dotted line represents the gold standard of FCS 0.143.*

Next neighbour analysis

To describe the organisation of ribosomes, vectors were calculated pointing from the centre of mass of one ribosome to one of its neighbours', i.e., the coordinates of the centre ribosomes were subtracted from its neighbour's coordinates. The vector was rotated by the transposed matrix of RELION's rotation angles to find the relative position of the neighbour. The particles sharing a similar arrangement to a neighbour were found in the same cluster.

Results

An extra density is observed on the ribosomal 30S subunit

In general, hibernating ribosomes are found in cells which are in stationary phase to save energy in order to survive. To gain insights into the mechanism of ribosome hibernation in archaea, we collected data in stationary phase. In our case, the cells are in the stationary phase at a cultivation time of 14 hours (Fig. S2).

To determine the 3D structure of the *P. furiosus* ribosomes, we performed cryo-electron tomography (cryoET). Tomograms were reconstructed from 2D images of a frozen hydrated sample obtained by a transmission electron microscope (TEM). The resolution of a tomogram is limited by the electron dose[31] that was applied. Therefore the contrast of the tomograms is low which makes it difficult to visually identify ribosomes. 70S particles could be observed in tomograms, which were binned 8 times to enhance the contrast and to save storage space (Fig. 1A). Subsequently, template matching was performed and the subtomograms were aligned in a completely unsupervised manner using an iterative, reference-free refinement algorithm for 3D images (Fig. 1B). This procedure verified the identification of ribosomes in our dataset.

Next, aligned particles were compared against each other and similar particles were clustered into groups, or classes. Particles sorted into well-resolved classes are separated from other particles that were sorted into poorly resolved or "junk" classes. Another round of refinement only containing the well resolved classes resulted in a 10.7 Å resolution structure. (Fig. 1C, 1E). Fitting the crystal structure derived from a *P. furiosus* ribosome in the density map revealed an additional density around the 30S subunit (Fig. 1C). local resolution map of this structure indicated low resolution for this additional density, suggesting it is either of low abundance or flexible (Fig. 1D).

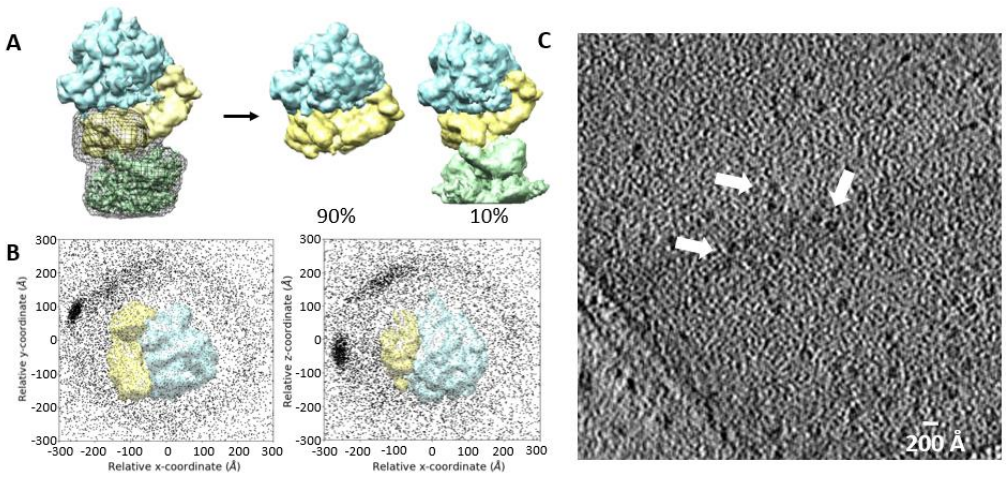

Figure 2, The extra density originates from dimeric ribosome structures. A. *3D classification on the extra density part and a part of the 30S subunit yielded two classes. The majority of the particles lack the extra density. B. Closest neighbour analysis. The centre-to-centre distance for each ribosome towards its closest neighbours is calculated. Left: x-y dimension, Right: x,z-dimension. C. . slice of a tomogram from the lamellae dataset. Tomogram was binned 8 times. Scale bar: 200 Å*

The extra density originates from a subset of hibernating ribosomes

To identify the origin of the extra density, classification was performed with a mask around the extra density and part of the 30S subunit (Fig. S3A). This yielded a class (90%) of particles lacking the extra density and a class (10%) of particles containing this extra density (Fig. 2A). As expected from the local resolution map (Fig. 1D), the amount of particles exhibiting this extra density is relatively low.

To prove if this extra density belongs to an attaching ribosome, we performed an analysis of next neighbour positions. In this analysis, the centre-to-centre distance of each ribosome to its neighbouring ribosomes was calculated and plotted. This analysis provided a quantification of the spatial organization of ribosomes. One densely populated cluster was observed in the 3D distribution at a relative x coordinate of approximately 300 Å, a relative y coordinate of approximately 100 Å and a relative z coordinate of approximately 0 Å (Fig. 2B). The observation of one cluster suggests that the position of the neighbouring ribosomes is the same with respect to each other, which is characteristic for dimeric hibernating ribosomes. This is different than what is observed in next neighbourhood analysis of polysomes in bacterial and human cells. For polysomes multiple clusters were observed, which indicates that the relative position of the ribosomes in a polysome conformation is not the same with respect to each other [32,33]. This is due to the fact that polysome particles have neighbours on multiple sites. The average centre-to-centre distance which can be deduced from the cluster in the plots is ~270 Å, which is approximately the size of a ribosome [34].

Additional evidence for ribosome dimers resulted from the observation of possible ribosome dimer structures in the tomogram (Fig. 1C). The extra density observed around the SSU could thus be assigned to part of another ribosome in a hibernating dimer conformation. The distribution of ribosome dimers in our dataset is in agreement with a previous study focusing on hibernating ribosomes *in situ* in *E.coli* cells, where it was found that 10 – 20% of the ribosomes in cells grown to stationary phase have a spatial arrangement characteristic of hibernating ribosome dimers [18].

Monomeric ribosomes represent translation elongation intermediate states

In order to capture the native states of the ribosome in *P.furiosus*, we did further classification of the classes containing dimeric ribosomes and monomeric ribosomes (Fig S3B, S3C). Classification with a mask around the ribosome part of the monomeric ribosome particles revealed five well resolved ribosome states that belong to the translation elongation cycle (Fig S3B, Fig. 3A). These states were characterised by the movement of tRNAs through the A-, P- and E-sites and the dynamics of the L1 stalk. The pre-translocation complex is represented by the most populated class showing densities for A-site tRNA and P-site tRNA. Studies have shown that E-site tRNA disassociates quickly after translocation[35] which involves the dynamics of the L1 stalk[36]. Here, we see that the classes containing densities for P-site tRNA and E-site tRNA are less abundant, suggesting E-site tRNA is less stable. 3% of the particles belonged to a class only containing the LSU (Fig. S4).

An additional density was observed in some classes originating from both monomeric and dimeric ribosomes. A ribosome structure from *P. furiosus* (PDB entry 4V6U) was used to fit in the density map of one of those classes (Fig. 3C). It is likely that this density belongs to an elongation factor. Elongation factors normally bind to the ribosome near the A-site and facilitate translational elongation during protein synthesis. Furthermore, studies have shown that translocation of bacterial and eukaryotic is accompanied by intersubunit rotation[37,38]. Surprisingly, we did not found any rotation in our classes.

Classification of the dimeric ribosome particles, revealed one well resolved class containing a density for E-site tRNA and the extra density near the A-site. (Fig. S3C, Fig. 3B). The observation of only one class suggests that the hibernating dimeric ribosome structures are in a fixed conformation. Elongation factor 2 (EF2) has been found to associate with eukaryotic and bacterial hibernating ribosomes[21,23]. A structure of EF2 (PDB entry 2EFG) was fitted in the extra density to see if EF2 is associated with archaeal hibernating ribosomes (Fig. S5). The structure

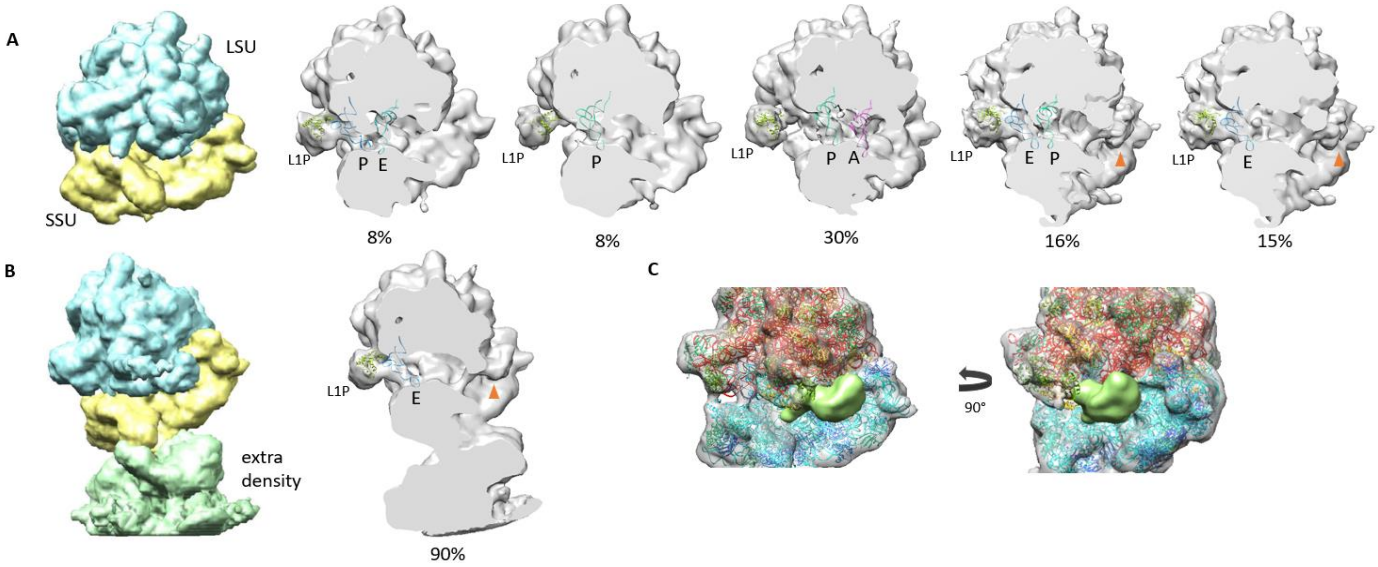

Figure 3, different states of native ribosomes *A. five classes from the monomeric ribosome particles with a resolution below 20 Å. The structure derived from 4V6U of the L1P subunit(green), E-tRNA(blue), P-tRNA(turquoise), A-tRNA(magenta) are fitted inside the densities of the different classes. Orange arrow indicates an extra density near the A-tRNA site. The percentages indicate the amount of particles within a class. B. one class from the dimeric ribosome particles with a resolution below 20 Å. The structures derived from 4V6U of the L1P subunit(green), E-tRNA(blue), P-tRNA(turquoise), A-tRNA(magenta) are fitted inside the densities of the different classes. Orange arrow indicates an extra density near the A-tRNA site. The percentage indicates the amount of particles within a class. C. The ribosome class derived from the particles with extra density. The density map is fitted with PDB entry 4V6U. The extra density is shown in green.*

fitted well, however still some amino acids were located outside the density.

A larger box size reveals surrounding densities

To better understand the structure of the hibernating ribosome dimer, the box size of the subtomograms was enlarged. This was achieved by binning the subtomograms 6 times to a pixel size of 13 Å. Initial 3D auto refinement of these subtomograms was performed and we were able to capture the entire ribosome dimer (Fig. S6A). In the refined structure of the 100S ribosome, the two faces of the 30S subunits are connected (Fig. 4A). Classification with a mask around the ribosome dimer structure shown in Fig. 4A revealed two distinct classes with a maximum resolution of 40Å (Fig S6B, Fig 4B). 16% of the particles belong to a class characterizing the ribosome dimer structure. This percentage is similar to the percentage of particles containing an extra density around the SSU shown previously. Furthermore, the other class consisted of a ribosome with two additional less resolved densities. One additional density appeared near the SSU and the other appeared near the mRNA exit site. The structure of this class average resembles the structure of an averaged 3D density of polysomes[32]. This comparison suggest that these densities could belong to attaching ribosomes in a polysome conformation. However, since these densities are poorly resolved, we expect that polysomes are not very abundant in the stationary phase of archaeal cells.

Several ribosomal proteins are involved in the contact region between the small subunits of the dimers (Fig 4C). Two main contact sites could be identified in the dimer interface. One contact site is formed by the interaction of L7AE proteins. L7AE is a protein that interacts with kink turn motifs in RNA and is present in multiple copies in archaeal ribosomes[8]. Two L7AE copies bind to the LSU, whereas one L7AE copy binds to the SSU. The L7AE

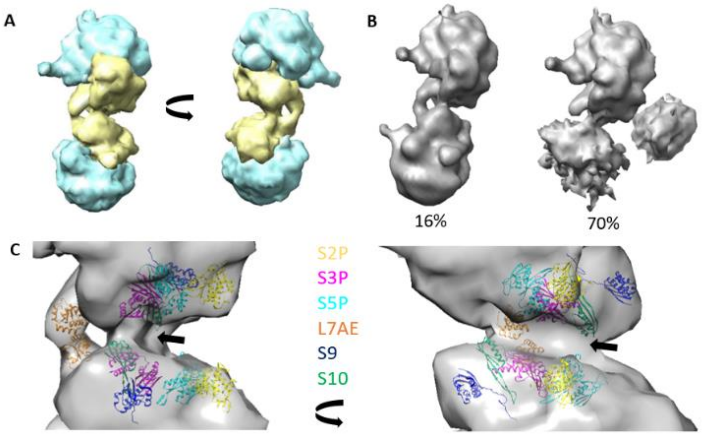

Figure. 4, structure of ribosome dimers. A. The averaged 100S ribosome density map with the arrangement of the large (blue) and small (yellow) subunits in the dimer found in stationary cells. B. Docking of the *P. furiusus* 70S ribosome structure (PDB entry 4V6U) into the two ribosomal particles of the ribosome dimer. C. Classification of the ribosome dimer structure revealed two classes. One class containing the hibernating dimeric ribosome particles (16%) and the other class showing additional density around the ribosome.

form the SSU interacts with another L7AE on the neighbouring SSU in a dimeric conformation. This promiscuity is specific for archaea and since this protein is present only on the large subunit of eukaryotic and bacterial proteins, we suggest that this binding site in the dimeric hibernating ribosome structure is also archaeal specific. There is also an additional density between the two SSUs (Fig 4C, arrowhead). At the present resolution, it was not possible to assign any hibernation factors as being associated with the ribosome dimer.

Comparison of *P. furiosus* dimer and bacterial dimers

To obtain more information on how our archaeal hibernating ribosome dimer deviates from its bacterial counterparts *S. aureus, E. coli and S. subtilis.* each structure was superimposed with the 100S *P. furiosus* structure. The orientation of our structure to its bacterial counterparts differs by a rotation of 45, 13 and 37° respectively (Fig. 5). The difference in angle among the 100S ribosomes from different bacteria is due to the mechanism of the hibernation factors. In *E.coli* RMF and short HPF cooperatively stimulate dimerization of 70S monomers by inducing the formation of 90S particles[39]. In *S. aureus and S. subtilis,* ribosome dimers are produced by RMF and long HPF and without the formation of an intermediate 90S dimer[40,41]. Since the *P. furiosus* 100S dimer most resembles the structure of *E.coli*, the mechanism of dimer formation might also be most similar to what has been observed in *E. coli*.

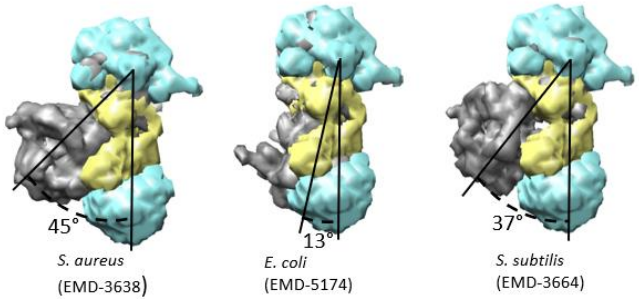

Figure. 5 Comparison of multiple 100S particle orientations with respect to the P. furiosus 100S ribosome. *The 100S particle structure from P. furiosus is coloured and oriented as shown in the right structure in Fig. 4A. Cryo-EM maps for E. coli (EMD-5174), S. subtilis (EMD-3664) and S. aureus (EMD-3638) were downloaded from the Electron Microscopy DataBank (EMDB). For each map, the pixel size was set to 13.02 Å and the box size to 100 pixels.*

Discussion

We used cryo-electron tomography to reveal the native state of ribosomes in the thermophilic archaeon *P. furiosus* in the stationary phase. The lack of knowledge in archaeal translation mechanism is primarily due to the difficulty in cultivating these organisms and because many archaeal model organisms are extremophiles, making it difficult to use classical biochemical and molecular methods. Thermophiles are organisms which can reproduce at high temperature by having specialized rigid enzymes which do not unfold at high temperature like most organisms[42].

Subtomogram averaging revealed a 10.7 Å resolution structure which fitted a crystal structure of a *P. furiosus* ribosome well. Additionally, we observed a poorly resolved extra density on the SSU (Fig. 1C, 1D). Subsequent classification revealed that this extra density was present in approximately 10% of the particles which explains why this density has a low local resolution (Fig. 2A). Using next neighbour analysis we determined that these originated from dimeric ribosome structures (Fig. 2B).

The majority of particles do not contain this extra density and classification of those particles revealed different states of the translation elongation cycle. The understanding of the elongation cycle of ribosomes in archaea remains limited. The native states of the elongation cycle determined here are comparable to a subset of sates of the elongation cycle determined in bacteria[43] and eukaryotes[44]. This observation suggests that even in stationary phase, there is still some translocation carried out by the ribosome. However, we did not observe any differences in the rotation of the SSU towards the LSU, which is normally observed in bacterial and eukaryotic ribosomes[37,38].

It was demonstrated that particles originating from the class containing ribosome particles have a single conformation with a density around the E-site tRNA and an additional density close to the A-site (Fig. 3B). It is observed in bacteria that ribosome hibernation induced conformational changes in the flexible domains, such as the L1 stalk, due to the interaction of hibernation factors[45]. A fixed conformation of the L1P subunit is also observed in dimeric hibernating ribosomes from eukaryotes[23]. This is mediated by a hibernating factor which exchanges with E-site tRNA and appears to lock the otherwise flexible P stalk into a fixed position to reduce its ability to promote polypeptide elongation and thus protein synthesis. Unfortunately, the resolution of our model is too low to identify if the E-tRNA site density is caused by a hibernating factor.

Apart from hibernating ribosome dimers, hibernating ribosomes from bacteria and eukaryotes can also stay in a monomeric conformation, in which hibernation factors block the active site of the ribosome[14,21,46]. Therefore it is possible that some classes that were classified from the monomeric ribosome particles, contain particles representing hibernating monomeric ribosomes. Since there is no information on the mechanism of hibernating ribosomes in archaea, additional research is needed to investigate this further.

We increased the pixel size to obtain more information on the surrounding densities and to capture the hibernating ribosome dimer as a whole. For the first time, an *in situ* structure of an archaeal hibernating ribosome dimer was reported (Fig. 4A). The dimer showed a head-to-head conformation connected by the two 30S subunits. An additional density was observed in between these two subunits. It is unlikely that the additional density is associated with a hibernation factors, since these factor mostly bind to the LSU close to the peptidyl transference centre[14]. Archaea are evolutionary more related to eukaryotes than bacteria, but the architecture of the dimer is similar to what is observed in bacteria (Fig. 5)[17,39].

Furthermore, we demonstrated that there is also a small population of polysomes in *P. furiosus* cells in the stationary phase. We do not know whether they are active but in the stationary phase, the population of polysomes is reduced[12,47]. In general, active ribosomes are thought to be rare in the stationary phase. Blocking tRNA binding sites in dimerized ribosomes might allow effective use of limited aminoacyl-tRNAs for the remaining active ribosomes. Thus, ribosome dimerization might play a role in facilitating protein synthesis under stress conditions by reducing competition for scarce resources.

Ribosomes normally do not form dimeric hibernating structures in cells which are in the exponential growth phase[18]. Furthermore, studies have shown that ribosome dimerization is reversible in bacteria[1639,40]. Thus 100S ribosomes are able to dissociate back into 70S ribosomes when cells are in normal conditions. In yeast, the Dom34-Hbs1 complex stimulates restart of translation after glucose starvation by dissociating inactive ribosomes[48]. Therefore, it would be interesting to investigate the ribosome structure of archaea in the exponential growth phase as well.

Ribosome dimerization might be conserved throughout the eukaryotic kingdom, including mammals. Recently the *in situ* structure of a eukaryotic hibernating ribosome dimer from the microsporidian species *S. lophii* was reported[23]. The architecture of this dimer is markedly distinct when compared to the archaeal 100S dimer and bacterial 100S dimers. This suggests that eukaryotic 100S ribosomes have a different dimerization mechanism than what is observed in bacteria and archaea so far. The open question remains how widespread hibernating ribosome dimers are amongst eukaryotes. Interestingly, one study demonstrated that hibernating ribosome dimers occur in rat glioma cells under amino acid starvation conditions[22].

In summary, we revealed a never-seen-before dimeric hibernating structure from archaea. Our experiments proved that only a subset of ribosomes form these dimeric ribosome structures. Additionally, we demonstrated that these ribosomes are in a uniform conformation compared to monomeric ribosomes. Interestingly, the structure of the archaeal dimeric ribosomes resembles the structure of bacterial ribosome dimers.

Acknowledgement

First, I would like to thank my supervisors Wenfei Song and Marten Chaillet for their support and guidance during the project. I learned a lot during this project about cryo electron tomography and especially data processing. I would also like to thank Friedrich Förster for providing me

with this opportunity. Last, I would like to thank the rest of the structural biology group for their suggestions and interesting discussions.

References

1. Steitz, T. A. A structural understanding of the dynamic ribosome machine. *Nature Reviews Molecular Cell Biology* vol. 9 242–253 (2008).
2. Aitken, C. E., Petrov, A. & Puglisi, J. D. Single ribosome dynamics and the mechanism of translation. *Annu Rev Biophys* **39**, 491–513 (2010).
3. Englmeier, R., Pfeffer, S. & Förster, F. Structure of the Human Mitochondrial Ribosome Studied in Situ by Cryoelectron Tomography. *Structure* **25**, 1574-1581.e2 (2017).
4. Cox, C. J., Foster, P. G., Hirt, R. P., Harris, S. R. & Embley, T. M. The archaebacterial origin of eukaryotes. *Proc Natl Acad Sci U S A* **105**, 20356–20361 (2008).
5. Londei, P. *et al.* Recent Advances in Archaeal Translation Initiation. *Frontiers in Microbiology | www.frontiersin.org* **1**, (2020).
6. Coureux, P. D., Lazennec-Schurdevin, C., Bourcier, S., Mechulam, Y. & Schmitt, E. Cryo-EM study of an archaeal 30S initiation complex gives insights into evolution of translation initiation. *Communications Biology* **3**, (2020).
7. Dennis, P. P. *Ancient Ciphers: Minireview Translation in Archaea*. *Cell* vol. 89 (1997).
8. Armache, J.-P. *et al.* Promiscuous behaviour of archaeal ribosomal proteins: Implications for eukaryotic ribosome evolution. doi:10.1093/nar/gks1259.
9. Lučić, V., Förster, F. & Baumeister, W. STRUCTURAL STUDIES BY ELECTRON TOMOGRAPHY: From Cells to Molecules. *http://dx.doi.org/10.1146/annurev.biochem.73.011303.074112* **74**, 833–865 (2005).
10. Buttgereit, F. & Brandt, M. D. A hierarchy of ATP-consuming processes in mammalian cells. *Biochem. J* **312**, 163 (1995).
11. Boucherie, H. Protein synthesis during transition and stationary phases under glucose limitation in Saccharomyces cerevisiae. *Journal of Bacteriology* **161**, 385–392 (1985).
12. Dickson, L. M. & Brown, A. J. P. mRNA translation in yeast during entry into stationary phase.
13. Mckay, S. L. & Portnoy, D. A. Ribosome Hibernation Facilitates Tolerance of Stationary-Phase Bacteria to Aminoglycosides. (2015) doi:10.1128/AAC.01532-15.
14. Prossliner, T., Skovbo Winther, K., Askvad Sørensen, M. & Gerdes, K. Ribosome Hibernation. *Annual Review of Genetics* 46 (2018) doi:10.1146/annurev-genet-120215.
15. Yoshida, H. *et al.* The Ribosome Modulation Factor (RMF) Binding Site on the 100S Ribosome of 'Escherichia coli 1. *J. Biochem* **132**, 983–989 (2002).
16. Ueta, M. *et al.* Role of HPF (Hibernation Promoting Factor) in Translational Activity in Escherichia coli. *The Journal of Biochemistry* **143**, 425–433 (2008).
17. Kato, T. *et al.* Structure of the 100S Ribosome in the Hibernation Stage Revealed by Electron Cryomicroscopy. *Structure* **18**, 719–724 (2010).
18. Ortiz, J. O. *et al.* Structure of hibernating ribosomes studied by cryoelectron tomography in vitro and in situ. *Journal of Cell Biology* **190**, 613–621 (2010).
19. Dyke, N. van, Chanchorn, E. & van Dyke, M. W. The Saccharomyces cerevisiae protein Stm1p facilitates ribosome preservation during quiescence. (2012) doi:10.1016/j.bbrc.2012.11.078.
20. Wang, Y. J. *et al.* Lso2 is a conserved ribosome-bound protein required for translational recovery in yeast. *PLOS Biology* **16**, e2005903 (2018).
21. Wells, J. N. *et al.* Structure and function of yeast Lso2 and human CCDC124 bound to hibernating ribosomes. (2020) doi:10.1371/journal.pbio.3000780.
22. Krokowski, D. *et al.* Characterization of hibernating ribosomes in mammalian cells. *Cell Cycle* **10**, 2691 (2011).
23. Mclaren, M. *et al.* In situ structure of a dimeric hibernating ribosome from a eukaryotic intracellular pathogen. doi:10.1101/2022.04.29.490036.
24. Mastronarde, D. N. Automated electron microscope tomography using robust prediction of specimen movements. *Journal of Structural Biology* **152**, 36–51 (2005).
25. Zheng, S. Q., Palovcak, E., Armache, J.-P., Cheng, Y. & Agard, D. A. Anisotropic Correction of Beam-induced Motion for Improved Single-particle Electron Cryo-microscopy. doi:10.1101/061960.
26. Kremer, J. R., Mastronarde, D. N. & McIntosh, J. R. Computer visualization of three-dimensional image

data using IMOD. *Journal of Structural Biology* **116**, 71–76 (1996).

27. Hrabe, T. *et al.* PyTom: A python-based toolbox for localization of macromolecules in cryo-electron tomograms and subtomogram analysis. (2011) doi:10.1016/j.jsb.2011.12.003.

28. Tegunov, D. & Cramer, P. Real-time cryo-electron microscopy data preprocessing with Warp. *Nature Methods* **16**, 1146–1152 (2019).

29. Zivanov, J., Nakane, T. & Scheres, S. H. W. A Bayesian approach to beam-induced motion correction in cryo-EM single-particle analysis. **6**, 5–17 (2019).

30. Pettersen, E. F. *et al.* UCSF Chimera—A visualization system for exploratory research and analysis. *Journal of Computational Chemistry* **25**, 1605–1612 (2004).

31. Henderson, R. The Potential and Limitations of Neutrons, Electrons and X-Rays for Atomic Resolution Microscopy of Unstained Biological Molecules. *Quarterly Reviews of Biophysics* **28**, 171–193 (1995).

32. Brandt, F. *et al.* The Native 3D Organization of Bacterial Polysomes. *Cell* **136**, 261–271 (2009).

33. Brandt, F., Carlson, L.-A., Hartl, F. U., Baumeister, W. & Grü Newald, K. Molecular Cell The Three-Dimensional Organization of Polyribosomes in Intact Human Cells. *MOLCEL* **39**, 560–569 (2010).

34. Londei, P. & Ferreira-Cerca, S. Ribosome Biogenesis in Archaea. *Frontiers in Microbiology* vol. 12 (2021).

35. Uemura, S. *et al.* Real-time tRNA transit on single translating ribosomes at codon resolution. *Nature* **464**, 1012–1017 (2010).

36. Trabuco, L. G. *et al.* The Role of L1 Stalk–tRNA Interaction in the Ribosome Elongation Cycle. *Journal of Molecular Biology* **402**, 741–760 (2010).

37. Guo, Z. & Noller, H. F. Rotation of the head of the 30S ribosomal subunit during mRNA translocation. *Proc Natl Acad Sci U S A* **109**, 20391–20394 (2012).

38. Freitas, F. C., Fuchs, G., Oliveira, R. J. de & Whitford, P. C. The dynamics of subunit rotation in a eukaryotic ribosome. *bioRxiv* 2021.04.19.440545 (2021) doi:10.1101/2021.04.19.440545.

39. Yoshida, H. & Wada, A. The 100S ribosome: ribosomal hibernation induced by stress. *Wiley Interdisciplinary Reviews: RNA* **5**, 723–732 (2014).

40. Khusainov, I. *et al.* Structures and dynamics of hibernating ribosomes from Staphylococcus aureus mediated by intermolecular interactions of HPF . *The EMBO Journal* **36**, 2073–2087 (2017).

41. Gohara, D. W. & Yap, M.-N. F. Survival of the drowsiest: the hibernating 100S ribosome in bacterial stress management. **64**, 753–760 (2018).

42. Kumar, S. & Nussinov, R. Review How do thermophilic proteins deal with heat? **. *CMLS, Cell. Mol. Life Sci* **58**, 1216–1233 (2001).

43. Xue, L. *et al.* Visualizing translation dynamics at atomic detail inside a bacterial cell. doi:10.1101/2021.12.18.473270.

44. Frank, J. The translation elongation cycle—Capturing multiple states by cryo-electron microscopy. *Philosophical Transactions of the Royal Society B: Biological Sciences* **372**, (2017).

45. Beckert, B. *et al.* Structure of a hibernating 100S ribosome reveals an inactive conformation of the ribosomal protein S1. doi:10.1038/s41564-018-0237-0.

46. Ehrenbolger, K. *et al.* Differences in structure and hibernation mechanism highlight diversification of the microsporidian ribosome. *PLOS Biology* **18**, e3000958 (2020).

47. Brengues, M., Teixeira, D. & Parker, R. Movement of Eukaryotic mRNAs Between Polysomes and Cytoplasmic Processing Bodies.

48. van den Elzen, A. M. G., Schuller, A., Green, R. & Séraphin, B. Dom34-Hbs1 mediated dissociation of inactive 80S ribosomes promotes restart of translation after stress. *The EMBO Journal* **33**, 265–276 (2014).

Supplementary

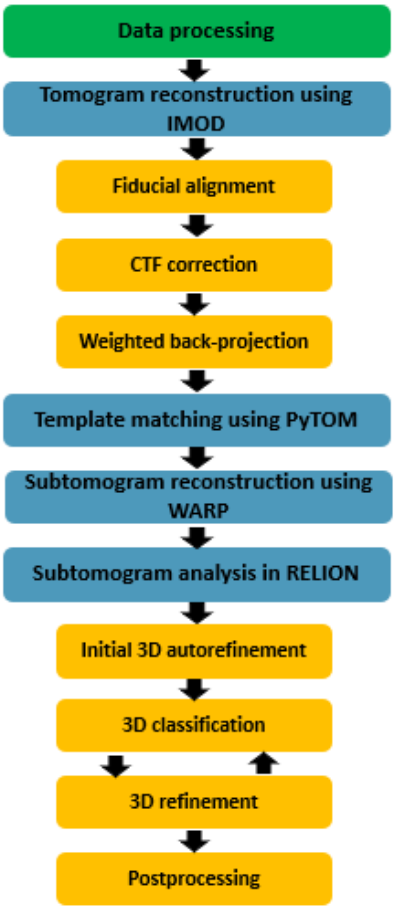

Figure S1, *Workflow of the image processing protocol. A schematic representation of the recommended workflow for subtomogram analysis. The software packages IMOD, PyTOM, WARP and RELION were used in this workflow (blue). Other crucial steps are depicted in yellow.*

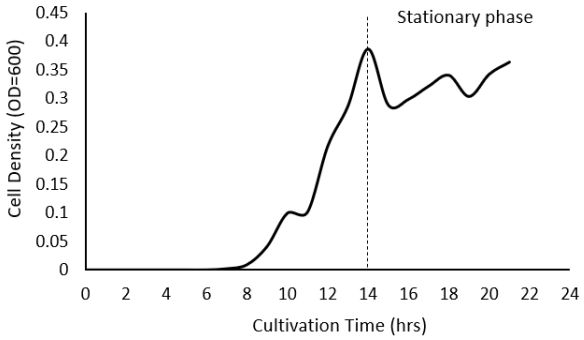

Figure S2, *Growth curve of Pyrococcus Furiosus. The optical density (OD) is measured every hour at 600 nm.*

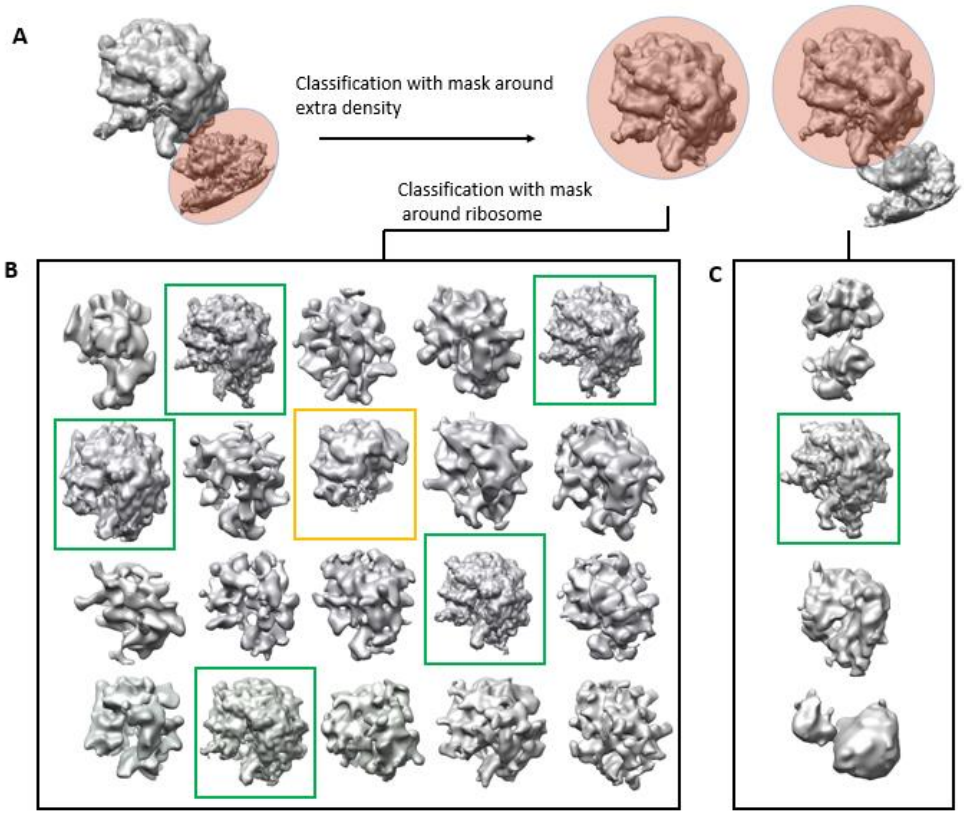

Figure S3, classification of ribosomes with and without extra density. *A. Classification with a mask around the extra density revealed two classes. One class containing particles with the extra density and one class containing particles without the extra density. B. Classification of the particles without the extra density, with a mask around the ribosome, revealed 20 classes. The well resolved classes (< 20 Å) are depicted by a green box. These classes were used for further identification. One class, depicted by the yellow box, only contained the 50S subunit. C. Classification of the particles with the extra density, using a mask around the ribosome, revealed 4 different classes. One class with a resolution < 20 Å is depicted by the green box.*

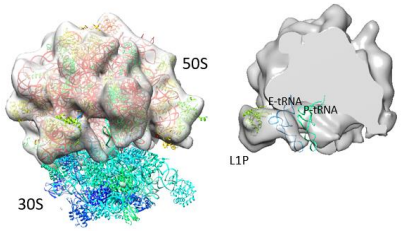

Figure S4, *50S subunit class. L1P interacts with the E-tRNA site. This class does not contain density for the P-tRNA site.*

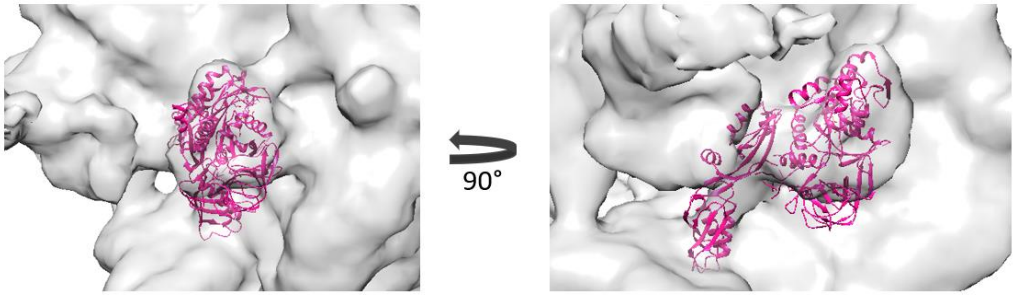

Figure S5, *Fitting the structure of EF2 (PDB entry 2EFG; pink) in the extra density near the A site.*

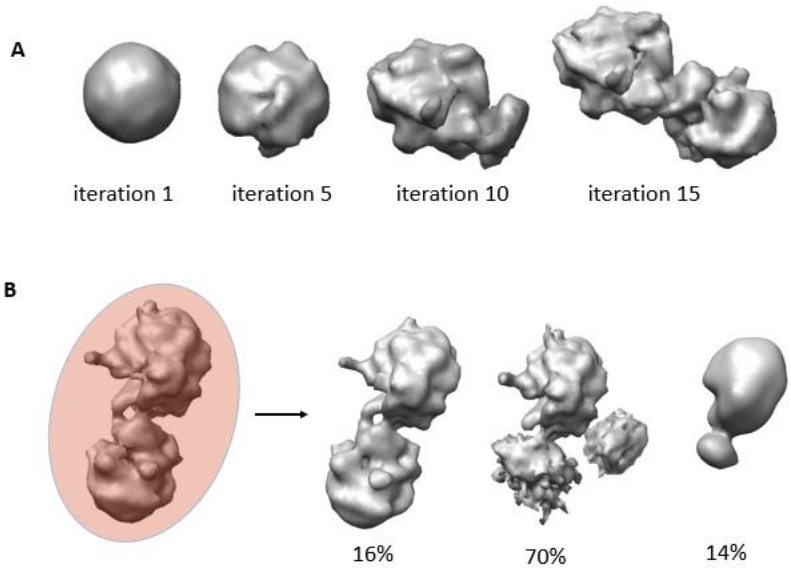

Figure S6, refinement and classification of hibernating rimer ribosomes. *A Representation of 3D maps obtained during iterative reference-free alignment of 6,407 sub tomograms. Iteration 1 corresponds to the initial reference that was obtained by averaging over all subtomograms in random orientations. B. Classification of the refined density map of a ribosome dimer. Classification yielded three classes. One class containing the hibernating dimeric ribosome particles (16%) , one class (70%) showing additional density around the ribosome and one "junk" class (14%).*

Script S1 *scripts used for template matching using the PyTOM package*

template_generation.py -f (template_file.mrc) -d (./your_directory) -o (output_file.mrc) -s (pixel size) -b (binning factor) --modify_structure --solvent_correction -x (missing wedge) -m -i

Layman's summary

A ribosome is an important complex molecular machine found inside the living cells that produce proteins from amino acids during a process called protein synthesis. The process of protein synthesis is a primary function, which is performed by all living cells. Without ribosomes, the human body would not be able to produce the proteins it needs to survive and would not function properly. Protein synthesis is one of the most energy demanding processes in the cell, so it is important that cells can regulate protein synthesis under different conditions. When cells encounter unfavourable conditions and cease to grow, ribosomes become inactive and protein synthesis is supressed to ensure the overall reduction of costly protein synthesis while maintaining a basal level of translation. This process is called ribosome hibernation and involves many proteins that inactivate the ribosomes. Studies have shown that hibernation can induce ribosomes to form ribosome dimers (a complex formed by two identical molecules that linked together). In this study we investigated ribosome hibernation in archaea. Archaea are a class of single-celled organisms with molecular characteristics that separates them from bacteria. Eukaryotes, for example cells from plants and animals, have likely been evolved from archaea. Hibernation is well studied in bacteria because of their simple system. Less is known about ribosome hibernation in eukaryotes since it is much more complex than in bacteria. In this study we use the archaeon *Pyrococcys Furiosus* which grows optimally at a 100°C. We use cryo- electron tomography (CET) to visualise ribosomes in these cells in their native state. In CET, a biological sample is flash frozen, thinned to an appropriate thickness, and then imaged using an electron microscope. The freezing process preserves the sample in a hydrated, native state. Multiple 2D images are captured as the sample is tilted along an axis and are computationally reconstructed to a 3D image called a tomogram. Using subtomogram averaging, copies of the same particle of interest within a tomogram are extracted independently (subtomograms) and then aligned and averaged to a common reference in order to increase the signal and detail of the underlying structure. Here, we imaged *P. furiosus* cells which are in the stationary phase, i.e cells that cease to grow due to unfavourable conditions, to capture the native state of ribosomes. Our results reveal the structure of hibernating ribosome dimers for the first time in archaea. Only a small subset of ribosomes formed hibernating ribosome dimers in *Pyrococcus furiosus*. Additionally we were able to capture native states of single ribosomes showing parts of the ribosome elongation cycle. For the dimeric ribosomes only one state was captured, suggesting that these ribosomes are in a single conformation. The overall structure of the dimer looked like the conformations previously seen in bacteria, but is not identical.